Shear dependence of particle pinch in JET L-mode plasmas

H. Weisen, A. Zabolotsky, X. Garbet[1], D. Mazon[1], L. Zabeo[1], H. Leggate[2], M. Valovic[2], K.-D. Zastrow[2] and contributors to the JET-EFDA work programme

Centre de Recherches en Physique des Plasmas
Association EURATOM-Confédération Suisse
École Polytechnique Fédérale de Lausanne, EPFL
CH-1015 Lausanne, Switzerland

[1)] CEA DRFC, Cadarache, France
[2)] UKAEA, Abingdon, UK

Abstract: The peakedness of the density profile in source-free MHD-quiescent L-mode plasmas with lower hybrid current drive (LHCD) is observed to decrease with decreasing peaking of the current profile. For the discharges investigated, which include normal and reversed magnetic shear plasmas, the relationship can be summarised as $n_{e0}/\langle n_e\rangle \cong 1.2 l_i$, where l_i is the normalised internal inductance. Density profiles are monotonically peaked at negative shear. Since density profiles remain peaked at zero loop voltage and negligible core particle source, the effect is attributed to an anomalous process of inward convection. No significant evidence was found for a correlation of density peaking with collisionality, nor of a dependence on temperature peaking within the parameter range investigated. The peaking of the temperature profiles and of the current profiles is uncorrelated in this dataset, allowing, for the first time, an experimental distinction between their effects on the density profile. The results are supportive of theories explaining particle convection by the anomalous curvature pinch or turbulent equipartition by trapped electrons, rather than by anomalous thermodiffusion.

1. Introduction

The nature of the inward particle pinch, which leads to the observed peaking of the density profile in tokamaks and stellarators, has been subject to controversy for a long time [1]. Recent experiments of fully current driven plasmas with negligible particle source in Tore Supra [1] and TCV [3],[4] have shown that substantial peaking is obtained in the absence of the Ware pinch [5] ($V_{Ware} \propto E_{tor}/B_{pol}$), providing an unambiguous demonstration of the

existence of anomalous pinches. Transport simulations for a variety of JET discharges have also concluded that an anomalous pinch must be present in the gradient zone ($r/a>0.5$), at least in L-mode plasmas [6]. The situation is more complicated in H-modes because sawteeth, ELMs, neutral beam fuelling and a significant Ware pinch contribute to the particle transport [6],[7]. The theoretical candidates for explaining anomalously high convection in the absence of the Ware pinch are turbulent equipartition (TEP) [8],[9],[10],[11],[12] or equivalently, it's fluid counterpart, the anomalous curvature pinch and anomalous thermodiffusion [13][14][15][16][17]. Neoclassical thermodiffusion [18] may only be expected in regions with strongly reduced anomalous particle diffusivity.

A substantial database modelling analysis of density peaking in Ohmic and ECH plasmas in TCV [3], which was based mainly of Ohmically relaxed, sawtoothing discharges, did not allow to determine which of TEP or anomalous thermodiffusion was the major contributor, because in these discharges the overall shear (or current profile peaking) remained correlated with the degree of peaking of the electron temperature profile, as well as with the sawtooth inversion radius, all of which scale with current profile peaking parameter $\langle j\rangle/(j_0 q_0)$, where $\langle j\rangle = I_p/A$ is the cross-sectional average toroidal current density, $j_0 q_0 = 2(1+\kappa_0^2)B_0/(\mu_0 \kappa_0 R_0)$, j_0, q_0 κ_0, B_0, and R_0 are the axial current density, safety factor, elongation, toroidal field and major radius [19][20]. The parameter $\langle j\rangle/(j_0 q_0)$ is the generalisation to arbitrary plasma shape of the historical scaling parameter $1/q_a$, (q_a being the safety factor at the last closed flux surface,) which describes profile peaking in sawoothing tokamak discharges with circular cross section [21]. Since in sawtoothing plasmas q_0 is approximately unity, we hypothesised that $\langle j\rangle/j_0$ rather than $\langle j\rangle/(j_0 q_0)$ would be the more general scaling parameter. For a given plasma shape $\langle j\rangle/j_0$ is proportional to q_0/q_{95}, where q_{95} is the safety factor at 95% of the poloidal flux between the magnetic axis and the last closed flux surface.

The sawtooth-free lower hybrid current driven (LHCD) JET L-mode discharges, described in part 2 of the paper, produced a range of current profiles for a fixed value of $\langle j\rangle/(j_0 q_0)$. These profiles are very different from those accessible in sawtoothing regimes, and span the range from normal shear to substantially reversed shear. They allow us test whether the peaking of the density profile follows the peaking of the current profile, as expected for TEP, or whether it follows the electron temperature profile, as expected for anomalous thermodiffusion. In part 3, the current status of the ongoing theoretical work on

anomalous particle transport is summarized and confronted with the observations. In part 4, the density profiles of the experiment are then modelled using a simple expression based on the most robust theoretical elements available to date.

2. Experimental observation of density peaking

The data for this study were obtained from a series of lower hybrid current driven (LHCD) L-mode discharges in JET, with LHCD powers in the range 0 (Ohmic) to 3.65 MW, part of which were produced to demonstrate safety factor profile control using the JET real time control system [22]. Full current drive with $V_{loop} \cong 0$ was obtained at the highest powers available, as shown in the example of fig.1, for otherwise similar discharges with $q_{95} \cong 8$, $0.8 \times 10^{19} m^{-3} \le \langle n_e \rangle \le 1.4 \times 10^{19} m^{-3}$ and central electron temperatures in the range $1.7 keV \le T_e(0) \le 6.3 keV$. LHCD drives an off-axis current, thereby broadening the current profile and for sufficient power, producing a hollow current profile [22]. This range of LH powers allowed the creation of a variety of magnetic shear profiles, ranging from normal at low power to strongly reversed at the highest power levels. Examples of the corresponding safety factor profiles are shown in fig.2 and were obtained by EFIT equilibrium reconstructions, which used Faraday rotation data from the JET interfero-polarimeter as a constraint [24]. Some of the discharges also had a small amount (<5MW) of centrally deposited ICRH heating. Despite having reversed shear profiles, these plasmas did not produce internal transport barriers, presumably because of the lack of centrally deposited auxiliary power. Electron temperature and density profiles from LIDAR Thomson Scattering (LTS), normalised to the central values, are shown in figs.3 and 4 and appear to be little or not affected by the differences in shear. The profiles shown are averaged over 1 second in stationary conditions in order to improve the rather poor signal-to-noise ratio of the LTS diagnostic at these low densities, for which uncertainties on individual data points are some 20%.

The continuity equation for the particle density $n=n_{e,i}$ can be expressed as $\frac{\partial n}{\partial t} = -\nabla(Vn - D\nabla n) + S$, where $-D\nabla n$ and Vn are diffusive and convective fluxes respectively and S is the particle source. Both the diffusive and the convective fluxes may be of neoclassical or of anomalous origin, although anomalous fluxes are generally much larger. Since no neutral beam injection was used in these plasmas, the only particle source is due to edge fuelling. The penetration of neutrals from the edge was calculated using the Kn1D code [25]. By radially integrating the above particle source, the source term $\Gamma_s(r) = \int_a^r S dr'$ can

directly be compared to the flux terms, as shown in fig.5 (solid line). Since particle fuelling is localised to the outer 10% of the cross section, it is immediately apparent that the particle source cannot explain the observed density gradients. Note that we have conservatively assumed that $T_i=T_e$. Since in these purely electron heated plasmas $T_i<T_e$, this leads to an overestimate of the penetration depth by successive charge exchange reactions.

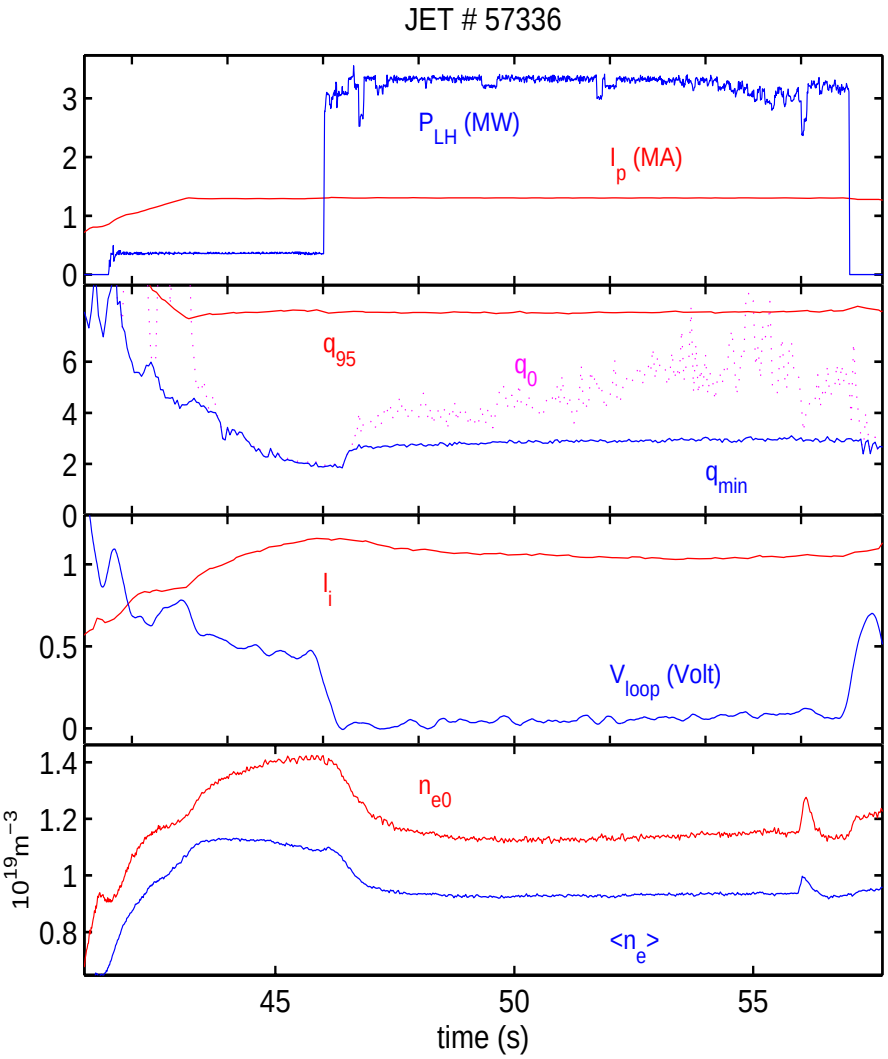

Fig. 1 Evolution of a JET LHCD discharge with $V_{loop}\cong 0$.

Top pane:time dependence of plasma current and LH power

Second pane:q_{95}, axial safety factor and minimum of safety factor profile from polarimetry

Third pane: Internal inductance and toroidal loop voltage

Bottom pane:Axial and average electron densities from interferometry

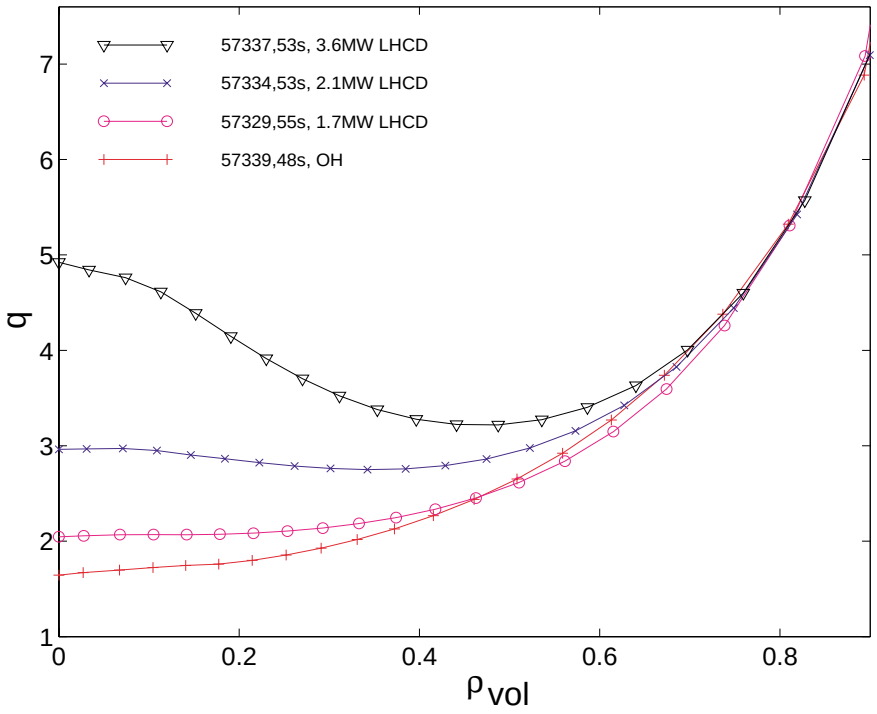

Fig. 2 Safety factor profiles from interfero-polarimetry, obtained with different levels of LHCD

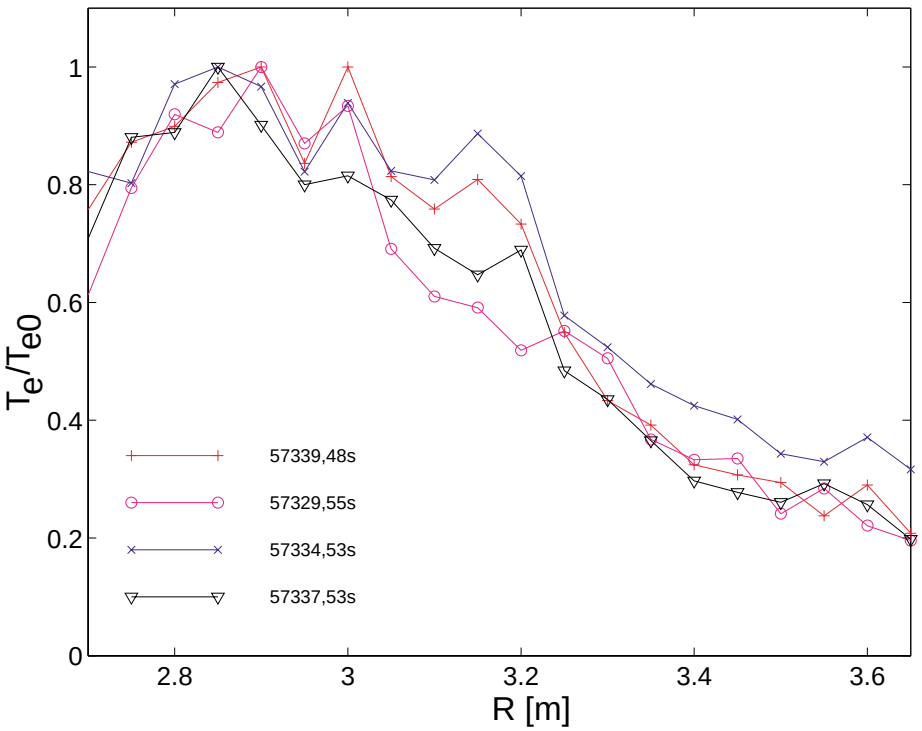

Fig. 3 Electron temperature profiles from LIDAR Thomson scattering corresponding to times in fig.2, averaged over 0.8s. Error bars on individual measurements are some 20%. The magnetic axis is at R≅2.95m.

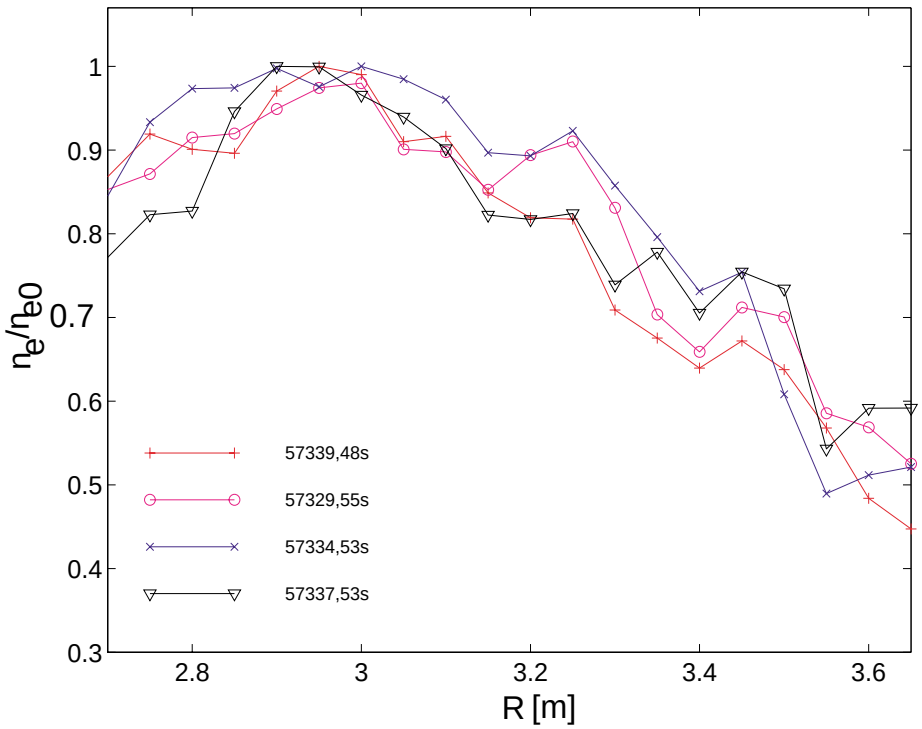

Fig. 4 Electron density profiles from LIDAR Thomson scattering corresponding to times in fig.2, averaged over 0.8s. Error bars on individual measurements are some 20%.

The fact that the absolute value of the flux is not known is unimportant as long as we are only interested in profile shapes. This allows us to undertake the following *Gedankenexperiment*: We assume that there is no convection and that the source term has to balance the diffusive flux. Realistic profiles for D, used to model particle and impurity transport in wide variety of situations, range from quadratic in minor radius, as assumed in fig.5, to flat (see e.g. [26]). We see that if the diffusive flux is assumed to be balanced in steady state by the source term near the plasma edge, this cannot, by a large margin, be the case in the bulk of the discharge. In fig.5 (broken lines) we have estimated the diffusive flux by assuming D=1m^2/s at the edge, a value typical for particle transport experiments [26]. (The exact value is not important for the above argument). If the diffusivity profile were flat, the discrepancy would be larger still. Hence in the bulk of the discharge the density profile in steady state must result from a balance of diffusion and convection, such that $\nabla n/n = V/D$. The fact that the density profiles remain peaked for $V_{loop} \cong 0$ also shows that a pinch mechanism other than the Ware pinch must be responsible.

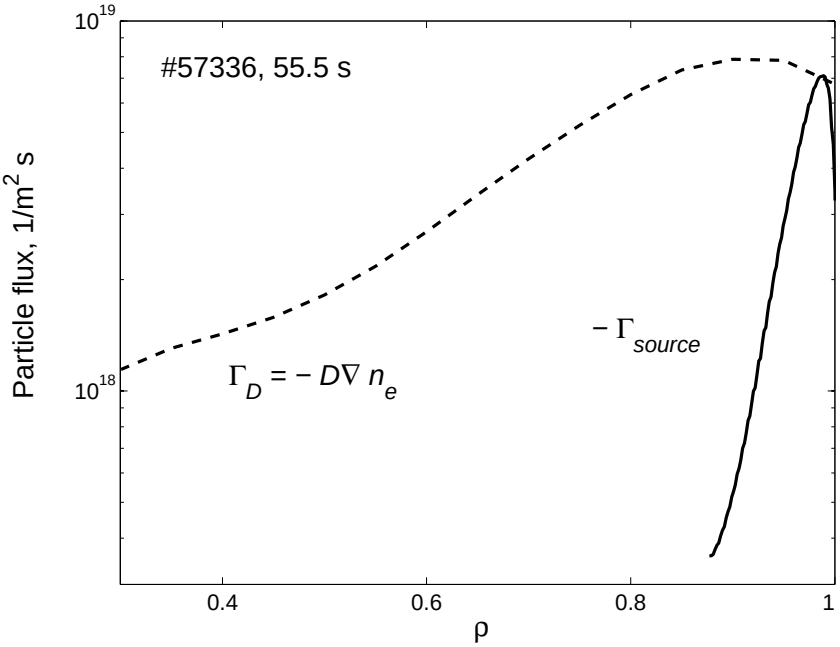

Fig. 5 Comparison of the radial profiles of the particle source term (-) and of the estimated diffusive particle flux (--), assuming $D=(r/a)^2$ [m^2/s].

In order to search for systematic dependencies, the data from these experiments were used to assemble a profile database of some 100 timeslices in quasi-stationary conditions with constant $\langle j\rangle/(j_0 q_0)$. Despite averaging the data over 1 second to reduce statistical noise, LTS profiles remained too noisy to serve as a reliable indicator for density profile changes. Instead, we used a peaking factor $\langle n_e\rangle/n_{e0}$, where $\langle\ldots\rangle$ is a volume average, derived from far infrared interferometry on JET, using an Abel inversion based on the shape of the magnetic flux surfaces. This definition of peaking factor (or profile width), corresponds, for monotonic profiles, to values between 0 and 1.

Fig.6 shows, as expected for TEP, that for constant $\langle j\rangle/(j_0 q_0)$, density peaking depends on overall shear expressed as $\langle j\rangle/j_0$ in normal shear plasmas defined by $q_{min}=q_0$. The relationship can be expressed approximately as $\langle n_e\rangle/(n_{e0}) \approx 0.25 + 1.67\langle j\rangle/j_0$. The symbol types in the figure refer to electron temperature peaking $\langle T_e\rangle/T_{e0}$ from LTS, showing, that within the range of variation of this parameter, no dependence is discernible in the dataset. In fig.7 we have plotted $\langle n_e\rangle/n_{e0}$ as a function of a qualitative indicator of temperature peaking determined from electron cyclotron emission, confirming that there is no correlation with temperature peaking. This indicator was chosen as the normalised temperature difference between the core and a point at 60% of the minor radius. ECE signals beyond some 65% of the minor radius were overwhelmed by downshifted radiation from LHCD generated suprathermal

electrons. The symbols in fig.7 are for classes of $\langle j\rangle/j_0$, showing that there is no correlation between $\langle j\rangle/j_0$ and $\langle T_e\rangle/T_{e0}$, which would allow the results to be interpreted either by TEP or by thermodiffusion.

When reversed shear discharges are included in the analysis, $\langle j\rangle/j_0$ ceases to be a suitable scaling parameter, fig. 8, as already expected from the observation that the central portions of the density profiles are insensitive to shear reversal (fig.4). The various symbols in fig.8 refer to classes of the reversal parameter q_{min}/q_0, as determined using the real time polarimeter inversion routines of the JET real time control system JET [27]. The best data alignment is obtained with the internal inductance, l_i, which can be determined independently from the equilibrium reconstruction. As a filter for data quality, the present dataset was restricted to reconstructions which yielded values for l_i, which up a systematic deviation (0.1), were consistent with the evaluation based only on the corresponding Shafranov integral. In order to conserve the appearance of fig.7 and for consistency with ref.[3], we have plotted $\langle n_e\rangle/n_{e0}$ versus $1/l_i$ in fig.9. We are not aware of any *a priori* theoretical reason for the good correlation $\langle n_e\rangle/n_{e0} \approx 0.83/l_i$ with this particular measure of current profile peakedness. (It should also be noted that the proportionality factor is expected to depend on plasma shape.)

The possibility of a visually unnoticed dependence of density peaking on temperature gradient lengths has been assessed using a three-parameter regression of the form $\langle n_e\rangle/n_{e0} = c_l/l_i + c_T\Delta T_e/\langle T_e\rangle + c_0$, where $\Delta T_e/\langle T_e\rangle$ was evaluated between $r=0$ and $r=0.6a$ as in fig.7. (The correlation coefficient for the deviations of $1/l_i$ and $\Delta T_e/\langle T_e\rangle$ from their mean values is *0.016*, i.e. the two regression variables are uncorrelated.) The result, $c_l=0.70\pm0.06$, $c_T=0.05\pm0.03$, $c_0=0.07\pm0.06$, with intervals given for the 90% confidence level, confirms that the dependence of density peaking on temperature peaking is very weak and borders on statistical insignificance.

Since the Abel inversion may in principle be prone to systematic errors, we cross checked this dependence using a qualitative but sensitive measure of peaking based on the ratio of the directly measured line average densities from a central and an off-axis interferometer chord. This is only applicable for a dataset with the same plasma geometry, as is the case here. Both chords are nearly horizontal, making them also insensitive to possible changes in core geometry caused by small differences in the Shafranov shift. The result in fig.10 shows that the chord ratio follows $1/l_i$ in the same way as the peaking factor derived from the Abel inversion. This figure is also resolved into classes of average electron density, showing that the absolute

density, which determines the depth of neutral penetration, has no effect on the peakedness of the density profile.

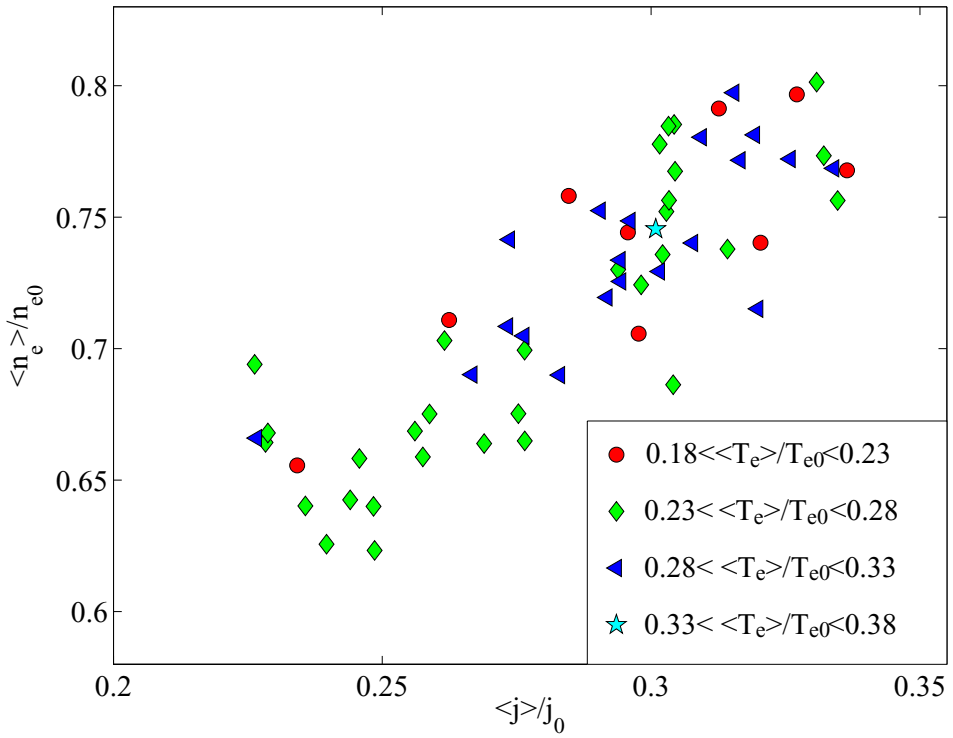

Fig. 6 Dependence of density peaking on the peaking of the current profile at constant q_{95} in normal shear discharges. Symbols refer to classes of electron temperature profile peaking parameter.

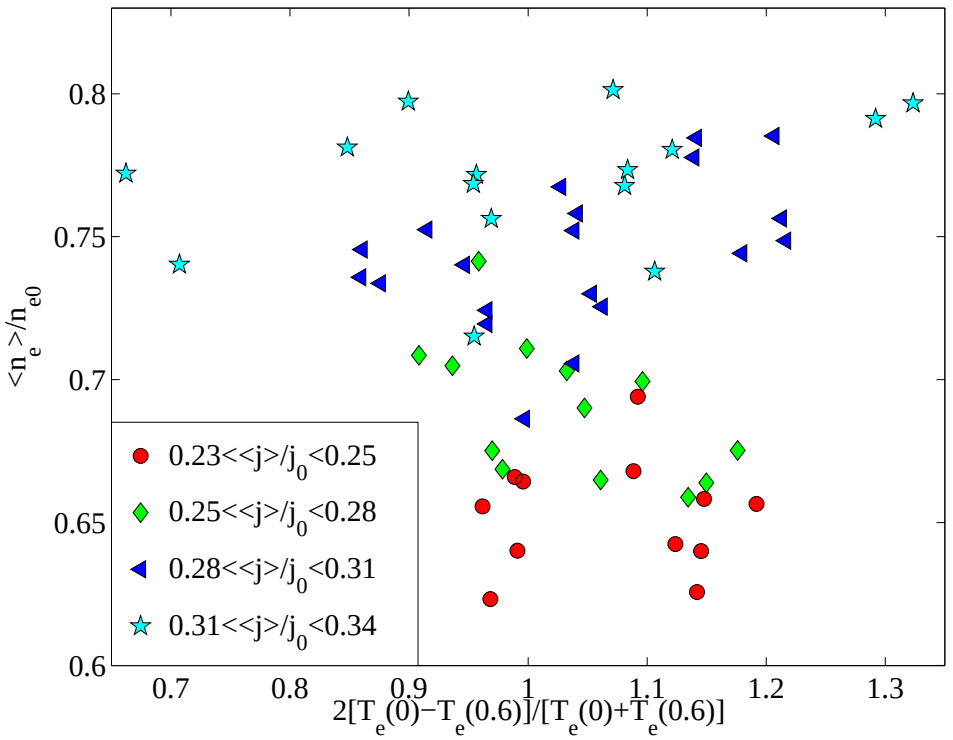

Fig. 7 Density peaking versus average electron temperature gradient from ECE in the plasma core region. Symbols refer to classes of current profile peaking.

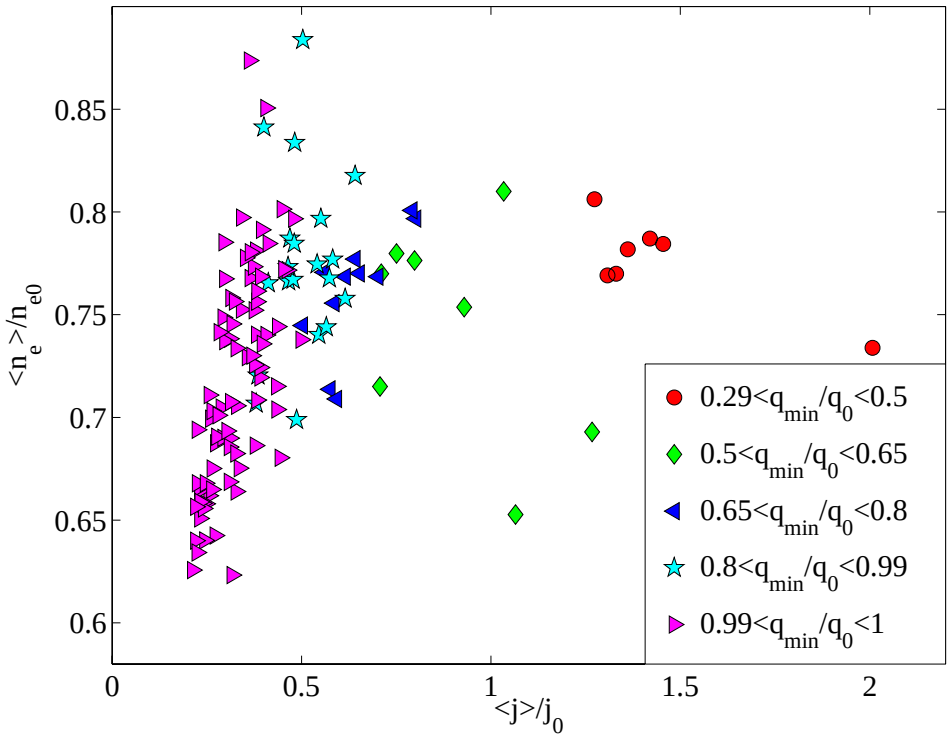

Fig. 8 Electron density peaking versus current density peaking (normal and reversed shear)

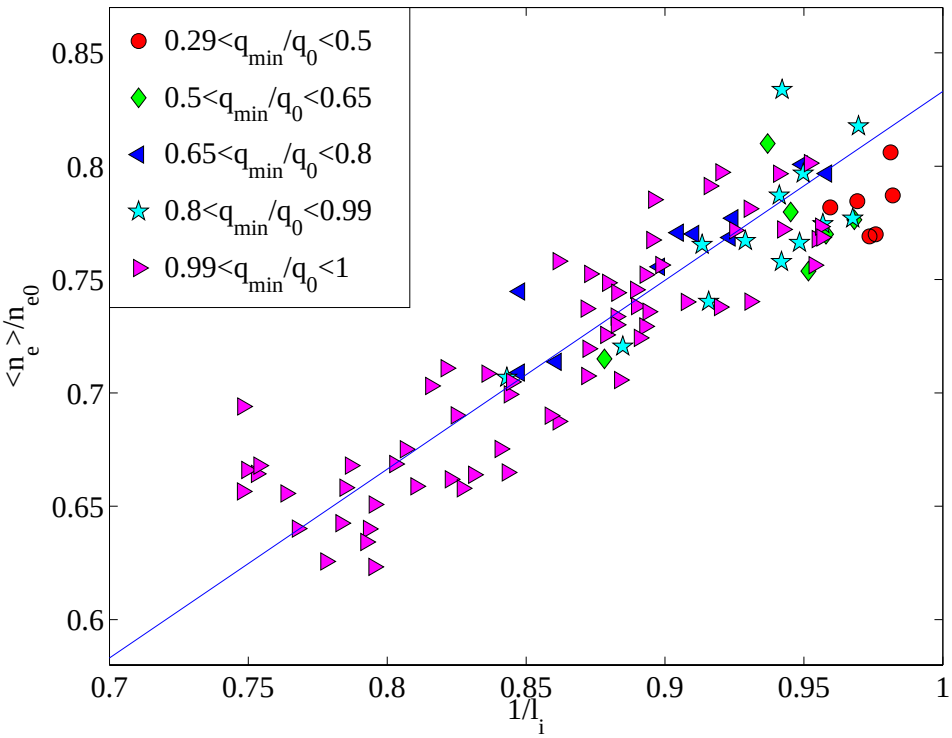

Fig. 9 Dependence of density peaking on internal inductance. Symbols refer to reversal parameter.

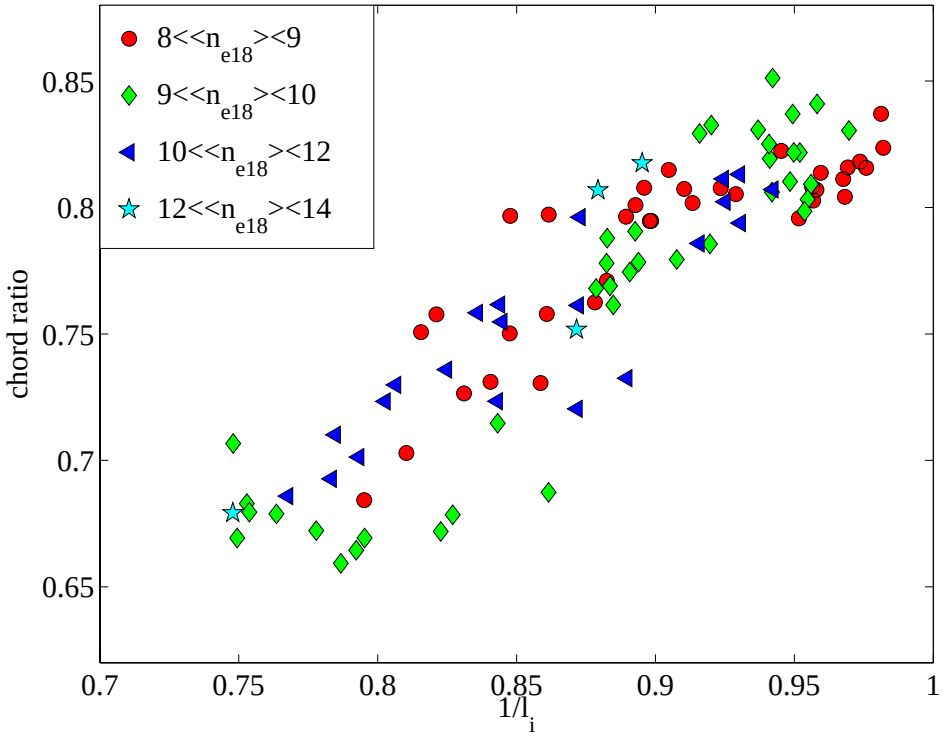

Fig. 10 Ratio of chord #5 (off-axis) and chord #8 (on-axis) line density measurement versus $1/l_i$.

The following figures show that, once the dependence on l_i is acknowledged, the loop voltage (fig.11), the LHCD power (fig.12) and the effective collisionality ν_{eff} (fig.13, introduced in the next section) have no further influence, although all three are of course correlated with l_i. The visual assessment is backed up by a further regression on the residuals of the aforementioned fit, $\langle n_e \rangle / n_{e0}\big|_{fit} = c_l / l_i + c_T \Delta T_e / \langle T_e \rangle + c_0$, showing that within 90% confidence there is no correlation of the deviation $\langle n_e \rangle / n_{e0}\big|_{fit} - \langle n_e \rangle / n_{e0}\big|_{experiment}$ of the density peaking factor with V_{loop}, LHCD power, q_{min}/q_0 or ν_{eff}.

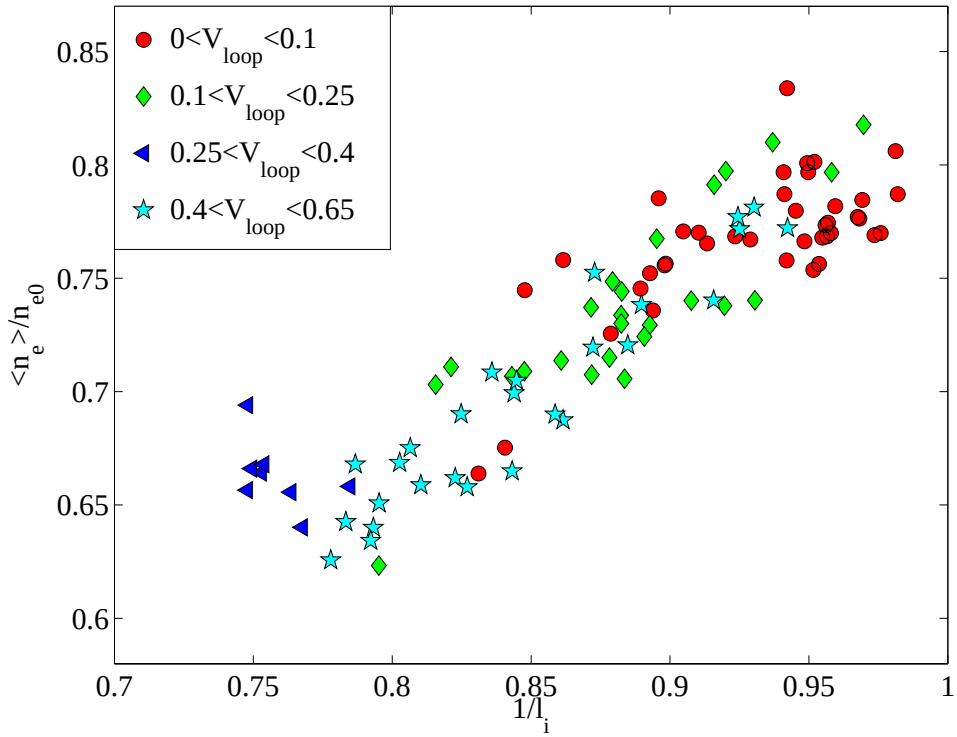

Fig. 11 Dependence of density peaking on internal inductance, resolved into classes of loop voltage.

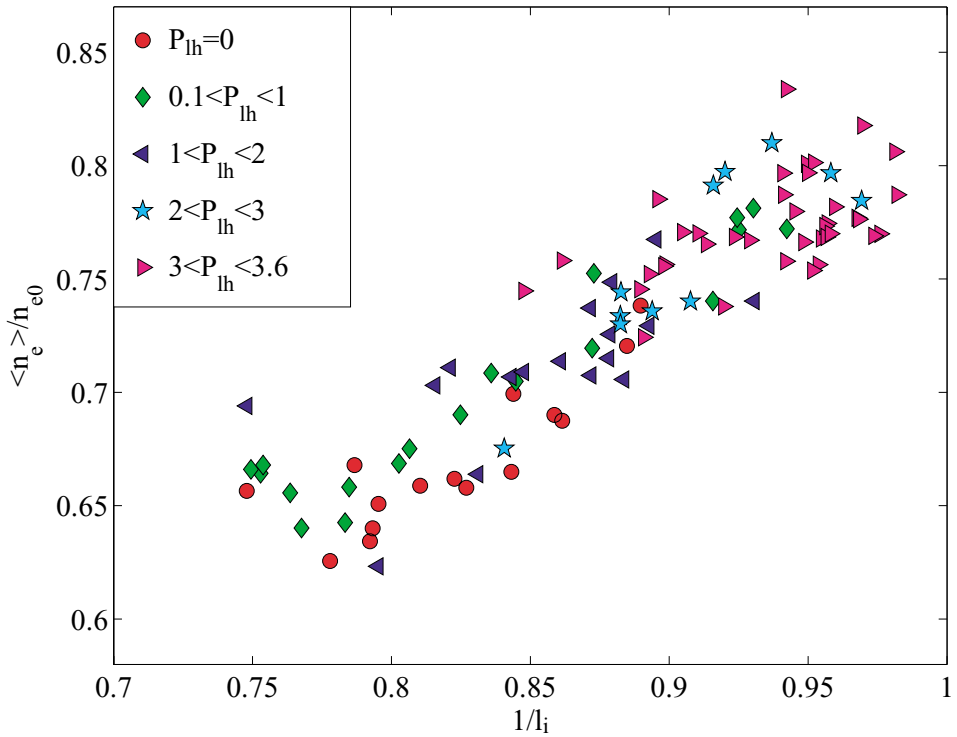

Fig. 12 Dependence of density peaking on internal inductance, resolved into classes of LHCD power.

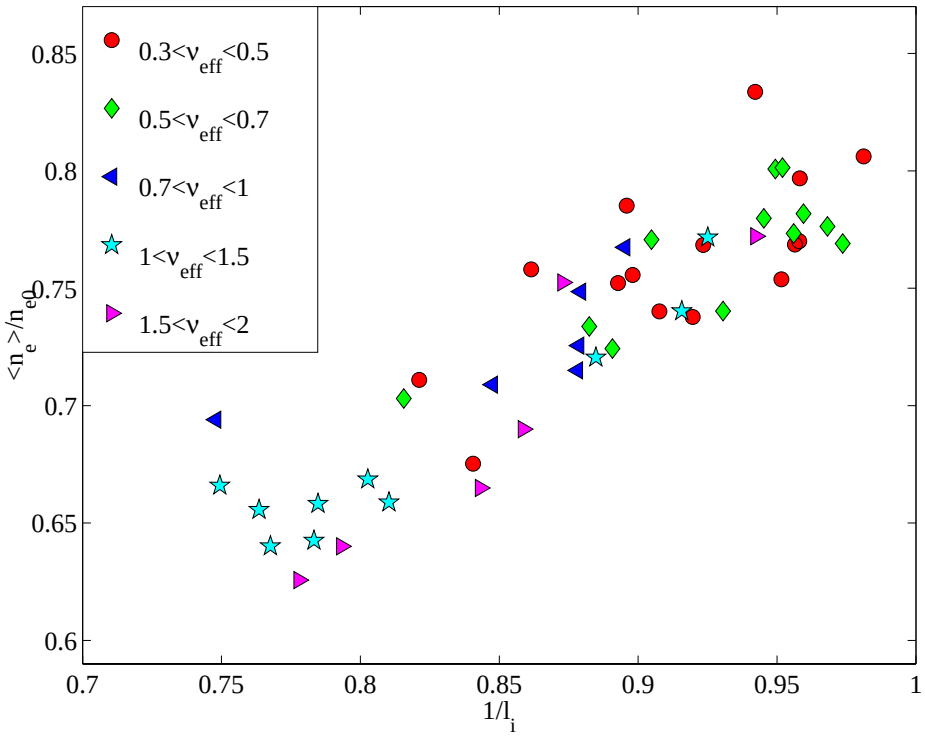

Fig. 13 Dependence of density peaking on internal inductance, resolved into classes of effective collisionality ν_{eff} at r/a=0.6. The electron collisionality ν ranged from 0.06 to 0.4.*

3. Comparison with theoretical predictions

The theoretical understanding of anomalous pinch processes, although still incomplete, has made considerable progress over the past decade. We can distinguish between two lines of theoretical investigation, which have led to testable predictions on the characteristics of the density profile. The first of these, referred to as 'turbulent equipartition theories' (TEP), is based on single particle invariants of motion and aims at predicting the general features of the plasma profiles resulting from turbulent drift wave transport within the frame of kinetic theory, while making a minimum number of assumptions on the nature of the underlying instabilities [8][9][10][11][12]. The second line is represented by a range of fluid turbulence models [13][14][15][16][17], which make predictions on both heat and particle transport.

The first TEP predictions by Yankov et al [8][9] conjectured that the electron density profile should be approximately given by

$$n_e(r)/n_e(0) \approx q(0)/q(r) \qquad \text{eq.1}$$

This holds well in the TCV tokamak at low auxiliary heating power [3][20], but the predicted profiles are often too strongly peaked for larger devices like JET. Isichenko et al. [10] recognised that trapped electrons are most likely to be subject to transport driven by low

frequency drift wave turbulence, such as produced by ion temperature gradient instabilities (ITG) and trapped electron instabilities (TEM) and consequently restricted TEP to trapped electrons. The resulting profiles are broader and are approximated by [10]

$$\frac{n_e(r)}{n_e(0)} \approx \left\{ 1 - \frac{4}{3R_0} \int_0^r \left(\frac{d\ln q}{d\ln r} + \frac{3}{8} \right) dr' \right\} \qquad \text{eq.2}$$

for circular cross sections. These two conflicting early predictions were reconciled by Baker et al [11][12], who investigated TEP under the assumption that turbulent transport is pitch angle dependent. The predictions of eq.1 appears as a limiting case when passing and trapped electrons are transported equally, whilst eq.2 is appropriate when only trapped particles undergo turbulent transport. Unfortunately this theory introduces the pitch angle dependence of transport as a free parameter. It has however been suggested that profiles described by eq.1 may be characteristic of plasmas dominated by dissipative trapped electron modes, whilst those described by eq.2 may relate to ITG-dominated turbulent plasmas, with the general possibility of mixed turbulence, giving rise to density profiles intermediate to those given by the above equations [28].

Fluid turbulence codes do not in general provide convenient expressions of broad validity for immediate comparison with experimental data, nor do they directly provide quasilinear transport coefficients for a transport equation resolved into diffusive and convective terms in the familiar form below:

$$\frac{\Gamma_e}{n_e} = D\left\{ -\frac{\nabla n_e}{n_e} - \frac{\gamma}{R_0} - \eta\frac{\nabla q}{q} + \alpha_e\frac{\nabla T_e}{T_e} + \alpha_i\frac{\nabla T_i}{T_i} \right\} \quad \text{eq.(3)}$$

An assessment of the contributions of the different terms can however be obtained (rather tediously) over many code simulations by varying the input profiles for the fluid model calculations [17]. In eq.3 the coefficients γ and η are positive, whilst α_e and α_i may be either positive or negative, depending on the conditions [14][17]. The second and third right hand side terms originate from electron drifts in the inhomogeneous magnetic field of the tokamak (curvature drifts). As a recent analysis of the fluid equations for collisionless drift wave turbulence has shown, the diffusive term together with the curvature terms produce exactly the same steady-state density profiles as those of TEP in the limiting case when only trapped electrons undergo turbulent transport, i.e. $\gamma=1/2$ and $\eta=4r/(3R_0)$ for circular cross sections [14].

Predictions for the thermodiffusive terms (the 4th and 5th at the right hand side of eq.3) appear to be more model dependent, as well as dependent on plasma conditions, such as the ratio of electron temperature to ion temperature and the nature of the underlying instabilities (ITG or TEM). So far no general theoretical picture for anomalous thermodiffusive convection has emerged. While some results [14][16] suggest that thermodiffusive pinches can be comparable in magnitude to the curvature driven pinch, others suggest that the curvature pinch can be significantly stronger than the thermodiffusive pinches [17]. The effect of collisionality is another important issue. Some fluid calculations predict a disappearance of convective fluxes and a flattening of the density profiles for effective collisionalities $\nu_{eff} = \nu^*_{ei}/\omega_{De} \sim 3(m_i/m_e)^{1/2}\varepsilon^{3/2}\nu^*_{ei}/q \geq 1$, where ν^*_{ei} is the electron collisionality familiar from neoclassical theory, ω_{De} is the curvature drift frequency and ε the local aspect ratio [17].

The lack of a dependence of the density profiles on changes of the electron temperature profile in the experiments reported in this article suggests that thermodiffusive pinches are considerably smaller than the curvature pinch in the conditions of these experiments. On the other hand the good correlation with global measures of shear, such as $\langle j \rangle / j_0$ and l_i is generally supportive of the curvature pinch or, equivalently TEP. The peaking is however clearly weaker than predicted by eq.1. It is interesting to note that this dataset straddles a collisionality regime which is intermediate between collisionless and collisional. Effective collisionality typically increases by an order of magnitude between r/a=0.2 and r/a=0.9. From Fig. 13 we see that at r/a=0.6, the effective collisionality ν_{eff} ranges from 0.3 to 2, without any correlation with the degree of density peaking. This is the range over which density peaking has been reported to disappear completely in ASDEX-upgrade ELMy H-modes, in agreement with fluid modelling [17]. Peaked density profiles are observed in TCV over the entire accessible collisionality regime $0.1<\nu_{eff}<50$ [3][20]. Such contrasting behaviour remains a challenge for theory which is likely to require detailed modelling over the large variety of conditions encountered in the various fusion devices and different heating methods.

4. Modelling of the density profiles

We first modelled these density profiles semi-empirically by assuming a pinch velocity $V = -\eta D \nabla q/q$, as in ref.[3]. Since the peaking subsists at zero loop voltage and is insensitive to the electron temperature peaking, neither the Ware pinch, nor thermodiffusion

are considered here. The modelled peaking is in reasonable agreement for normal shear if $\eta \sim 0.4$, but fails to describe reversed shear plasmas, for which it predicts hollow density profiles, which are clearly outside the error bars of the LTS diagnostic.

The TEP profiles from eq.(2), however are in good agreement with the data (Fig. 14), producing a dependence on l_i which is close to the experimentally observed one. Eq.(2) doesn't produce hollow profiles, even in the cases with the strongest shear reversal. The model profiles were evaluated by replacing r with the volume coordinate $\sqrt{V/V_{tot}}a$ and using safety factor profiles from polarimeter constrained equilibrium reconstructions. The number of datapoints is smaller than in the previous figures because reconstructions with good polarimeter measurements were only obtained for a subset of the data.

Fig. 15 shows examples of model profiles produced using the above expression and the safety factor profiles shown in fig.2. The central part of the experimental profiles is somewhat more peaked than the model profiles, especially at reversed shear, suggesting that an additional peaking mechanism may have to be invoked in the plasma core. Although there is good agreement with TEP/curvature pinch predictions in positive shear regions, we must be aware that this should not necessarily be expected at low or negative shear. Anomalous pinches only exist as a result of microturbulence such as TEM and ITG modes. If these modes are suppressed or stabilised, as may be the case in regions with low or negative shear and with low core heating as with off-axis LHCD, the corresponding pinches would be absent too. In the discharges described here, this would still leave the weak neoclassical pinches other than the Ware pinch, such as neoclassical thermodiffusion for which $V_{Te,\,neo} = D_{neo}\nabla T_e/(2T_e)$ in axisymmetrical geometry [18]. In the absence of any other convective mechanism and anomalous diffusion, this pinch tends to produce density profiles such that $\nabla n_e/n_e = \nabla T_e/(2T_e)$. To test this hypothesis it would be necessary to confirm experimentally, or at least theoretically, that the low or reversed shear core region is turbulence-free, an undertaking which is beyond the scope of this paper.

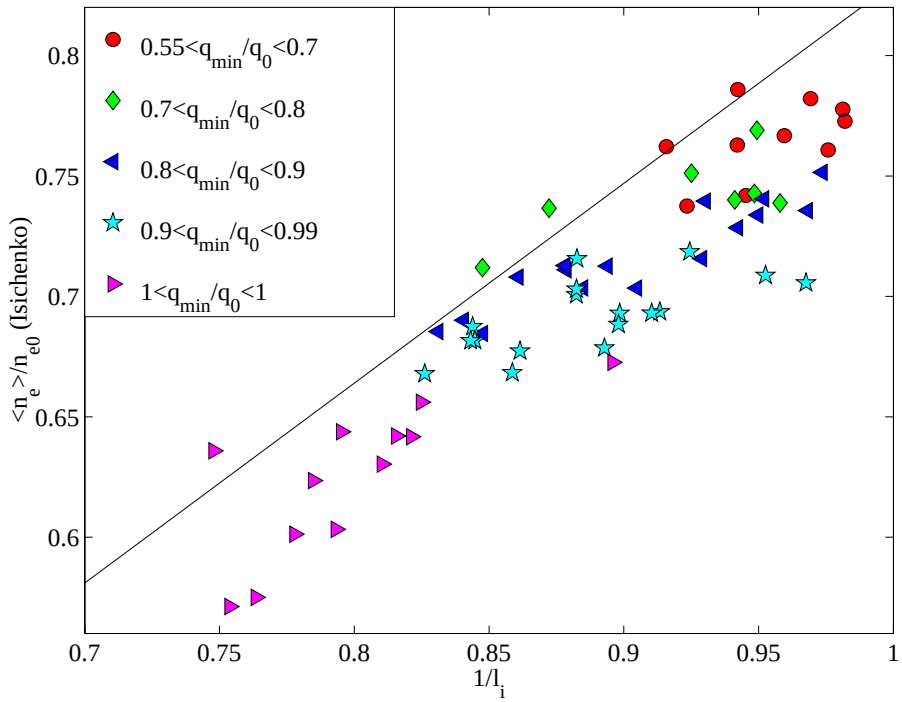

Fig. 14 Scaling with internal inductance of the density peaking factor evaluated using eq.2. Symbols refer to the reversal parameter. Safety factor profiles were taken from polarimeter-constrained equilibrium reconstructions. The line represents the average trend of the experimental data.

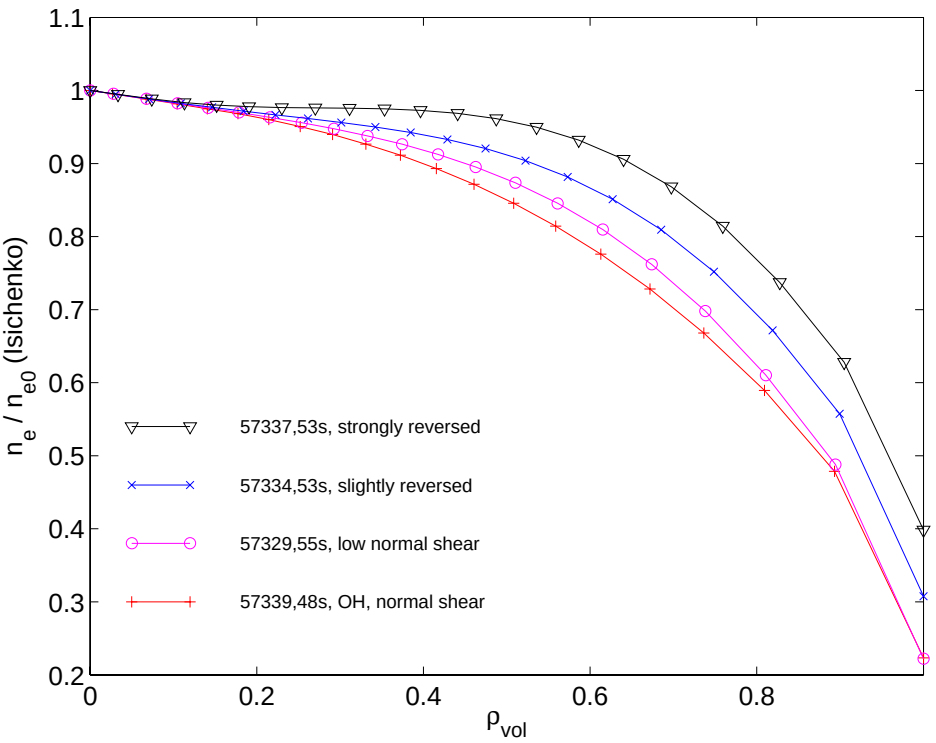

Fig. 15 Examples of density profiles from eq.(2), modelled using the safety factor profiles in Fig. 2.

5. Conclusions

In normal shear L-mode plasmas with fixed $q_{95} \cong 8$, the peaking of the density profiles is found to scale with the peaking of the current profile, $\langle n_e \rangle / n_{e0} \approx 0.25 + 1.67 \langle j \rangle / j_0$, with no significant dependence on the peaking of the electron temperature profile. A more general relation, $n_{e0} / \langle n_e \rangle \approx 1.2 l_i$, was found to applicable to both the positive and the negative magnetic shear plasmas in the dataset. Although the overall density profile follows responds to changes in the current profile, this is not the case in the core, which maintains a monotonic density profile at negative shear. A contribution from the Ware pinch can be excluded for the fully lower hybrid current driven plasmas in the dataset. Density peaking is also independent of effective collisionality in the range covered by these experiments, $0.3 < \nu_{eff} < 2$ for ν_{eff} evaluated at 60% of the minor radius.

Previous observations of the anomalous pinch [2][3][4] have not provided the answer to the question of the relative importance of TEP and anomalous thermodiffusion. The present LHCD experiments have clearly and for the first time, identified TEP, rather than anomalous thermodiffusion, as the dominant anomalous process of particle convection at normal shear. The density profiles are in fair agreement with simple model profiles proposed by TEP theory under the assumption that only trapped electrons contribute to the transport [10][11], as well as with fluid theory, if only the curvature pinch is considered [14]. For the discharges investigated, the model predicts a scaling of $n_{e0} / \langle n_e \rangle$ with the internal inductance l_i, which is very similar to the experimentally observed one.

Acknowledgements. The support of the entire JET-EFDA operating and diagnostics teams is gratefully acknowledged, as well as stimulating discussion with J. Weiland, V. Tokar, C. Angioni and J.B. Lister. We wish to thank B. Labombard for generously making the Kn1D code available. This work was partly supported by the Swiss National Science Fund.

References:

[1] F. Wagner and U. Stroth, *Plasma Phys. Control. Fusion* **35** (1993) 1321

[2]G.T. Hoang, C. Bourdelle, B. Pégourié, B. Schunke et al, *Phys. Rev. Lett.* **90** (2003) 155002

[3] A. Zabolotsky, H. Weisen, TCV Team, *Plasma Phys. Control. Fusion* **45** (2003) 735

[4] I. Furno, H. Weisen, TCV Team, *Physics of Plasmas* **10** *(*2003) 2422

[5] A.A.Ware, *Phys Rev. Letters* **25** (1970) 916

[6] L. Garzotti et al., *Nuclear Fusion* **43** (2003) 1829

[7] H. Weisen et al, *EFDA-JET preprint* 3053 (2003)
http://www.iop.org/Jet/fulltext/EFDP03053.PDF

[8] V.V. Yankov, *Plasma Physics Reports* **21** (1995) 719

[9] J Nycander and V.V. Yankov , *Phys. Plasmas* **2** (1995) 2874

[10] Isichenko M.B., Gruzinov A.V., Diamond P.H. and Yushmanov P.N., *Phys. Plasmas* **3** (1996) 1916

[11] D.R. Baker and M.N. Rosenbluth, *Phys. Plasmas* **5** (1998) 2936

[12] D.R. Baker et al., *Nuclear Fusion* **40** (2000) 1003

[13] X. Garbet et al., *Physical Review Letters* **91** (2003) 03500

[14] H. Nordman, J. Weiland, A Jarmen, *Nucl. Fusion* **30**, (1990) 983

[15] R. Waltz et al., *Physics of Plasmas* **4** (1997) 2482

[16] J. Weiland 'Collective modes in inhomogeneous plasmas' *IOP Publishing Ltd, 2000, Bristol & Philadelphia, ISBN 0 7503 0589 4 hbk*

[17] C. Angioni et al., *Physical Review Letters* **90** (2003) 205003

[18] L.M. Kovrizhnykh, *Nucl. Fusion* **24**, (1984) 851

[19] H. Weisen et al, *Physics of Plasmas* **6** (1999) 1

[20] H. Weisen et al, *Nucl. Fusion* **42** (2002) 136

[21] V. Arunasalam *et al.*, *Nuclear Fusion* **30** (1990) 2111

[22] D. Mazon et al, *Plasma Phys. Control. Fusion* **45** (2003) L47

[23] A. Ekedahl et al, *Nucl. Fusion* **38** (1998) 1397

[24] G. Braithwaite et al, *Rev. of Scient. Instrum*. **60**, 2825

[25] B. Labombard (MIT), *PSFC Research Report* **PSFC-RR-01-03** (2001)
http://www.psfc.mit.edu/library/01RR/01RR003/01RR003_full.pdf

[26] The JET Team, *Nucl. Fusion* **39** (1999) 1891

[27] L. Zabeo et al., *Plasma Phys. Control. Fusion* **44** (2002) 2483

[28] M.Z. Tokar et al., *Physical Review Letters* **84** (2000) 895